1162 | https://doi.org/10.3311/PPci.16483
Creative Commons Attribution

Periodica Polytechnica Civil Engineering, 64(4), pp. 1162–1169, 2020

Analysis of Seismic Fragility Functions of Highway Embankments

Balázs Hübner[1*], András Mahler[1]

[1] Department of Engineering Geology and Geotechnics, Faculty of Civil Engineering, Budapest University of Technology and Economics, Műegyetem rkp. 3., H-1111 Budapest, Hungary
[*] Corresponding author, e-mail: hubner.balazs@epito.bme.hu

Received: 18 May 2020, Accepted: 19 July 2020, Published online: 02 September 2020

Abstract

Vulnerability assessment of structures is a vitally important topic among earthquake engineering researchers. Generally, their primary focus is on the seismic performance of buildings. Less attention is paid to geotechnical structures, even though information about the performance of these structures (e.g. road embankments, levees, cuts) during an earthquake is essential for planning remediation and rescue efforts after disasters. In this paper the seismic fragility functions of a highway embankment are defined following an analytical methodolgy. The technique is a displacement-based evaluation of seismic vulnerability. Displacements of an embankment during a seismic event are approximated by a 2-D nonlinear ground response analysis using the finite element method. The numerical model was calibrated based on the results of a 1-D nonlinear ground response analysis. The expected displacements were calculated for 3 different embankment heights and Peak Ground Acceleration (PGA) values between 0,05 and 0,35g. Based on the results of the 2-D finite element analysis, the relationship between displacements and different seismic intensity measures (PGA, Arias-intensity) was investigated. Different damage states were considered, and the probability of their exceedance was investigated. The seismic fragility functions of the embankments were developed based on probability of exceedance of these different damage states based on a log-normal fragility function. The legitimacy of using a log-normal fragility function is also examined.

Keywords

ground response, earthquake, fragility function, embankment

1 Introduction

Fragility functions (curves) help describe the seismic performance of civil engineering structures at various levels of shaking intensity [1]. They are mostly used for the analysis and design of superstructures and nuclear structures [2, 3] and are seldom used to describe seismic performance of geotechnical structures, e.g. embankments and road cuts. The seismic design of these geotechnical structures is usually done with simplified, pseudo static methods and little attention is paid to numerical modelling. Although there are several recommendations for the fragility curves of different embankments, these are usually based on empirical and semi empirical methods [4,5]. To construct such a fragility curve, previous damage at or near the site have to be taken into account, which may prove difficult in moderately seismic regions, as there are usually little to no data regarding the intensity and damage of previous seismic events. To overcome these limitations, more emphasis has been paid to analytical fragility curves in the last decade. They can be developed for moderately seismic regions based on numerical simulations. In this paper, the seismic fragility curves of highway embankments with different geometries are constructed based on the methodology developed by Argyroudis and Kaynia [6]. Following the methodology, the probability of exceedance of different damage states is determined based on the displacements of the embankments calculated from a nonlinear 2-dimensional site-response analysis. The fragility curves are assumed to have a log-normal distribution; validated at the end of the study.

2 Determination of the fragility curves

The fragility curves are based on nonlinear seismic ground response analysis for a given site. Multiple embankments with different heights (3–6–9 m) and a 1:2 slope were analyzed.

Cite this article as: Hübner, B., Mahler, A. "Analysis of Seismic Fragility Functions of Highway Embankments", Periodica Polytechnica Civil Engineering, 64(4), pp. 1162–1169, 2020. https://doi.org/10.3311/PPci.16483

2.1 Soil strata

The site is located in Tehran, Iran. The strata were defined based on site investigations and laboratory tests. The soil profile was divided into two layers: an upper sandy silt, and a lean clay layer. The embankment was built from gravelly silty sand found in-situ. The soil parameters for each layer are summarized in Table 1.

To describe the dynamic properties of the soil, a 48 m deep down-hole test was performed, and a shear wave velocity profile generated (Fig. 1). The maximum shear wave velocity recorded during the test was 555 m/s. Measured velocity values are less than standard values [7] for bedrock (750 m/s). This means that the in-situ test did not reach the bedrock. We added a linear extrapolation to the data from 48 m depth to a depth where velocity reached 750 m/s. Using this methodology, the depth of the bedrock was defined at 95 m. The soil strata can be classified as Soil Type III [7], based on the average measured shear wave velocity in the upper 30 meters of the strata. This classification is analogous to the Soil Type C defined in the Eurocode-8 [8].

The shear modulus for small strains can be determined for the profile based on shear wave velocities and unit weights of the layers using Eq. (1):

$$G = v_s^2 \rho. \tag{1}$$

Table 1 Soil parameters of the soil layers

Depth (m)	*PI (%)*	γ-γsat(%)	φ (°)	*c* (kPa)	*cu* (kPa)
0–24	8.2	20.0–21.0	24	30	-
24–48	15.6	20.0–21.0	32	28	40
Embankment	-	18.0–19.0	20	13	-

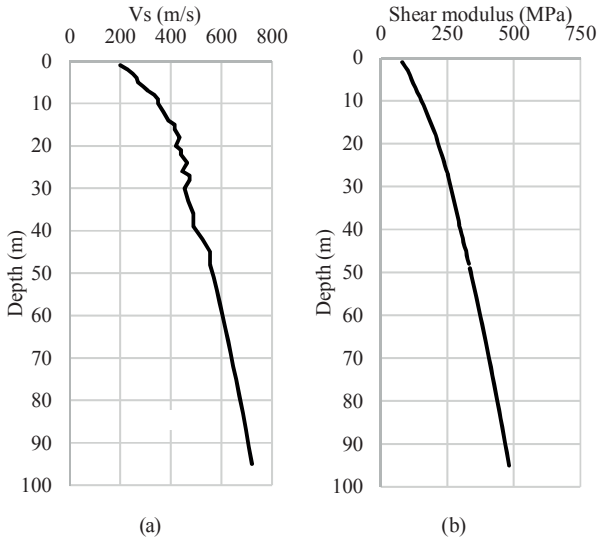

Fig. 1 a) Shear wave velocity, b) Shear modulus versus depth

2.2 Investigated earthquake records

The earthquake accelerograms for the ground response analysis were taken from the PEER [9] database. A total of six earthquake records were investigated (SMART1-25, 1983 (*Mw* = 6.50); San Fernando, 1971 (*Mw* = 6.61); Northridge-01, 1994 (*Mw* = 6.69); Kobe, 1995 (*Mw* = 6.90); SMART1-45, 1986 (*Mw* = 7.30); Manjil, 1990 (*Mw* = 7.37)), all of which had a moment magnitude over 6.50. The records are similar to earthquakes that occurred in the Tehran region in the past 20 years. The six accelerograms were recorded on Type I (bedrock, or EC-8 Type-A soils) soils, therefore no deconvolution analysis was needed to obtain the bedrock motions. Their acceleration spectra closely match the standard for Type I soil with 5 % damping ratio. The time-histories were further scaled to achieve PGA values 0.05 g–0.35 g in 0.05 g steps for use in later analyses. Arias-intensity and peak ground acceleration (PGA) were used to characterize the input accelerograms [10].

2.3 Ground response analysis

Embankment displacements were estimated by a 2-D time history analysis using the geotechnical finite element software, PLAXIS 2D. To verify the 2-D model, a 1-D nonlinear ground-response analysis was performed with Deepsoil 6.1 [11]. Damping ratios in the 2-D model were calibrated using results from the 1-D analysis. In both analyses displacements were calculated based on the Newmark-Beta integration scheme [12]. The scaled earthquake acceleration records were applied at the bottom boundary of the model as horizontal acceleration constraints. The analysis was carried out for the duration of the records.

2.3.1 1-D nonlinear ground response analysis

The 1-D response software used a shear modulus reduction curve and damping curve for each soil layer to describe the behavior for cyclic loading. The curves, developed by Darendeli [13], were based on the effective mean stress and plasticity index of the soils. Results from the 1-D analysis were used to calibrate the 2-D models. Acceleration histories at the surface and layer boundaries were used to adjust the small strain damping of the 2-D models by matching the accelerations and displacements. Fig. 2. shows the acceleration history at the surface and at 12.0 m depth for the San Fernando earthquake, used in the analysis.

2.3.2 2-D finite element analysis

To better evaluate the geometric effects of an embankment, a 2-D model was constructed using PLAXIS 2D.

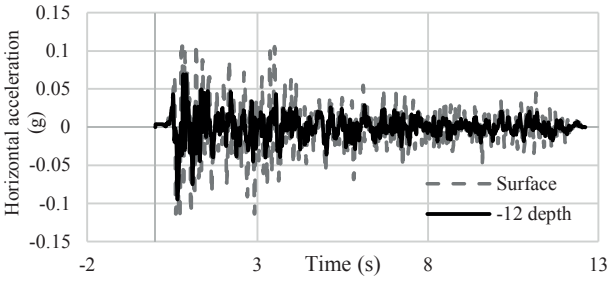

Fig. 2 Accelerations from the ground response analysis using the San Fernando earthquake (scaled to 0.10 g)

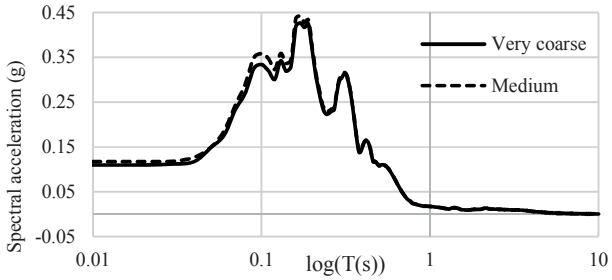

Fig. 3 Response spectra of the investigated point for 5 % damping ratio

The model boundaries were determined based on literature review. A compliant base boundary condition was used on the bottom boundary, which made it possible to apply a time-dependent acceleration constraint on the boundary. On the left and right sides of the model, a viscous boundary condition was applied, as recommended by PLAXIS. They reduce reflection and enable a reduced mesh while still achieving free field motions near model boundaries [14]

The horizontal size of the model was based on recommendations in literature as well. The width of the model was 1000 m and depth extended to 95 m resulting in acceptable depth ratio between 8–30 [15–17].

The typical element size was determined by Eq. (2) using the average shear wave velocity (V_s) of the soil column and the typical frequencies (f) of the earthquake records [18]. This produced an average element size less than 2.74 m.

$$L_{max} = V_s / \left(\left(5 \div 8 \right) \times f \right) \tag{2}$$

The restriction mentioned in Eq. (2) made the 2-D model very time consuming to compute, therefore a sensitivity analysis was made to determine the effect of the different mesh sizes to the displacements of the embankment. The results of the analysis are shown in Table 2.

The results show that doubling the average size has little effect on embankment crown displacement. Fig. 3 shows the response spectra of the same point for a 5 % damping ratio. It can be seen, that although the displacements did not change significantly, there was an observable attenuation in the higher frequency range part of the response spectra caused by change in the element size. Based on these results, a medium density finite element mesh was used for the analysis.

Table 2 Displacements of the left crown of the embankment using different mesh sizes.

Mesh definition	Avg. element size	Displacement [m]
Very coarse	5.024	0.005069
Coarse	3.535	0.004996
Medium	2.672	0.004996

For the 2-D finite element analysis, the Hardening Soil with small strain stiffness material model [19] was used. This model reproduces the small strain stiffness (G_0) as indicated by V_s profiles measured in the field (Fig. 1). The backbone curves of the soil layers are described by the small strain shear modulus (G_0^{ref}) at a reference stress level (p_{ref} = 100 kPa), and a treshold strain ($\gamma_{0.7}$) value. The modulus profile increases with the depth and can be represented using the reference shear modulus (G_0^{ref}), cohesion (c) and friction angle (φ), and exponent (m = 0.5–1.0, depending on soil type) as a function of depth (Eq. (3)):

$$G_0 = G_0^{ref} \left(\frac{c \cos\cos\varphi - \sigma_3^{'} \sin\sin\varphi}{c \cos\cos\varphi + p^{ref} \sin\sin\varphi} \right)^m . \tag{3}$$

The use of Eq. (3) allows for a refined mesh without redefining the soil layers. A single layer may have many G_0 values as deeper elements are subjected to higher confining stress (σ_3'). The soil parameters used in the finite element model are shown n Table 3.

Table 3 Soil parameters used in the finite element model

Soil properties	Embankment	Sandy silt	LP clay
g_{unsat} (kN/m^3)	18	20	20
g_{sat} (kN/m^3)	19	21	21
E_{oed}^{ref} (MPa)	7.000	25.000	27.000
E_{50}^{ref} (MPa)	7.000	25.000	27.000
E_{ur}^{ref} (MPa)	21.000	75.000	81.000
m (-)	0.5	0.80	0.55
c'^{ref} (kPa)	13	30	28
φ' (°)	20	24	32
ψ (°)	0	0	0
$\gamma_{0.7}$ (-)	0.0001	0.00025	0.001
G_0^{ref} (MPa)	87.500	170.000	180.000
OCR (-)	1.0	1.0	1.0

Although the HS small material model can generate a hysteretic material damping, experience shows, it is below the actual behavior at very small strains [20]. To approximate the real soil behavior, an additional damping has to be considered via the Rayleigh-formulation [21], by adding a frequency-dependent viscous damping to the material model. It can be described by three parameters: the damping ratio and two frequencies. At these two frequencies the Rayleigh damping is the prescribed damping ratio, between those frequencies the system is underdamped and above and below them it is overdamped. Various literature recommend the value of damping ratio to be between 0.5–2.0 % [22]. The first frequency used to describe the Rayleigh-damping formulation is taken as the fundamental frequency of the soil column. The second is based on the ratio of the fundamental frequency of the input acceleration and the natural frequency of the soil column, rounded to an odd integer. [22]. The natural frequency of the soil column can be approximated by Eq. (4), where f_s is the natural frequency of the soil column, T_s is the natural period of the soil column, $v_{s,avg}$ is the average shear wave velocity of the soil strata and H is the height of the soil column.

$$f_s = 1/T_s = v_{s,avg}/4H \tag{4}$$

The Rayleigh damping parameters were based on the above mentioned assumptions and equations. The damping ratio was calibrated from 1-D nonlinear results so that the free field displacements and accelerations from the 1-D analysis would match the results from the 2-D model. With an added damping ratio of 1 % the free field results of both analyses showed a good agreement.

2.3.3 Results

After the calibration of the 2-D model, the embankments were subjected to increasing seismic intensity and their displacements were recorded.

Ground response analyses were performed for three different embankment heights and six different acceleration histories, each scaled from 0.05 to 0.35 g. The results of the analysis using the San Fernando earthquake as input accelerograms are shown in Table 4. for each peak ground acceleration. The Arias-intensities belonging to the records is also shown in the table. Fig. 4. shows the results for the ground response analysis of the San Fernando earthquake record scaled to a peak ground acceleration of 0.05 g.

A relationship between the displacements and the seismic intensity was apparent from the results, and a power function in the following form was developed to describe their connection, where the Peak Ground Displacement (PGD) is the displacement of the embankment, α_{Int} is a coefficient of the seismic intensity and β_{Int} is the power of the seismic intensity.

$$PGD = \alpha_{Int} \cdot Intensity^{\beta_{Int}} \tag{5}$$

In case of a 9.0 m high embankment, the displacements can be determined with the following equation based on the PGA of the input acceleration.

$$PGD = 3.7151 \times PGA^{2.0004} \tag{6}$$

The relationship between the displacements and the seismic intensities are shown in Fig. 5 for the case of a 9.0 m high embankment. Similar relations were found for other embankment heights as well.

The relationship between the Arias-intensity and displacements was also investigated (Fig. 6). To describe the connection between these two parameters, Eq. (5) was used. While in case of the PGA a near-squared power function

Table 4 Displacements of the embankment's left crown

Earthquake	PGA (g)	Arias-intensity (m/s)	Embankment height (m) / Displacement (m)		
			9.0	6.0	3.0
San Fernando	0.05	0.02	0.005	0.003	0.002
	0.10	0.08	0.021	0.010	0.006
	0.15	0.15	0.039	0.018	0.008
	0.20	0.26	0.064	0.031	0.010
	0.25	0.40	0.082	0.049	0.012
	0.30	0.58	0.101	0.066	0.018
	0.35	0.79	0.121	0.081	0.025

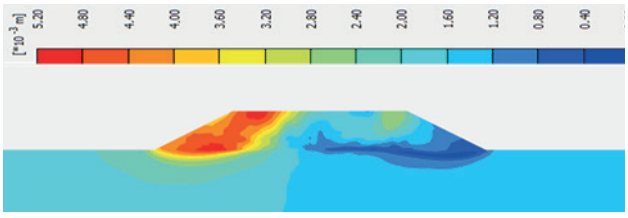

Fig. 4 Displacements of the embankment in case of the San Fernando earthquake (PGA =0.05 g)

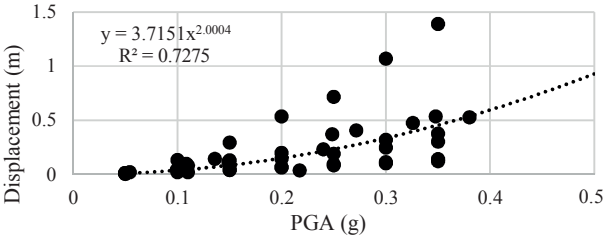

Fig. 5 Relationship between seismic intensity and displacements

described the relationship, for Arias-intensity, a near-linear correspondence was found between the displacements and intensity. Fig. 7 shows this relationship.

The parameters of Eq. (5) are summarized in Table 5. for different seismic intensities and different embankment heights. The variation of parameters with height of the embankment is shown in Fig. 8. A linear relationship can be found between the coefficient of the Arias-intensity and the embankment height.

$$\alpha_{Arias} = 0.0312 \times H - 0.0273 \tag{7}$$

As stated before, the exponent of the PGA function is very nearly 2.0 ($\beta_{PGA} = 2.0$), while in case of the Arias-intensity, a linear relationship ($\beta_{Arias} = 1.0$) can be found. For the coefficient of the *PGA* function, no such connection was found.

Based on Fig. 8. the parameters of Eq. (5) can be derived for different embankment heights, which can be used to derive the displacements of the embankments at a given seismic intensity.

2.4 Damage states

To define the fragility curves, the determination of damage states is needed. The fragility curve will describe the probability of exceedance of these damage states. Even though damage evaluation based on peak displacements is an accepted methodology, the boundaries between damage states varies between researchers [6, 23, 24]. For our analysis, the damage states for highway embankments suggested by Argyroudis and Kaynia [6] were applied. The damage states and their corresponding maximum and minimum Peak Ground Displacements (PGD) are shown in Table 6.

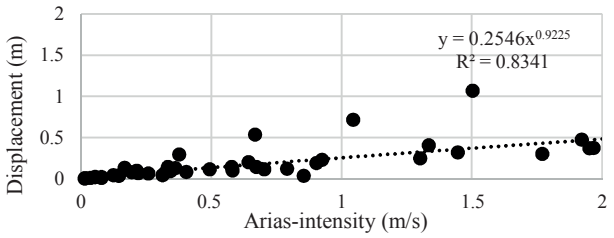

Fig. 6 Relationship between Arias-intensity and displacements

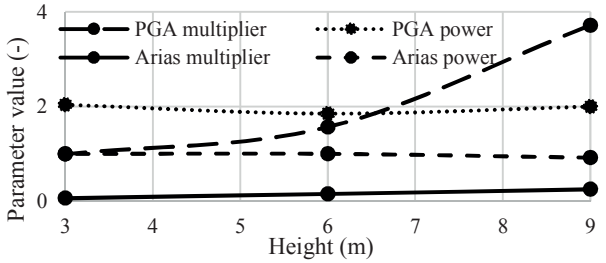

Fig. 7 Change of the parameters of Eq. (5) with increasing height

2.5 Development of the fragility curves

Fragility curves are usually defined with a lognormal distribution. This assumption was applied to our analysis to define probability of exceedance of the various damage states. The lognormal distribution is described with Eq. (8):

$$P(D > DS_k) = 1/2\left[1 + \Phi\left(\frac{\left(\ln\ln PGA - \ln\ln \mu\right)}{\beta\sqrt{2}}\right)\right]. \tag{8}$$

Where P is the probability of damage (D) higher than damage state "k" (DS_k), Φ is the standard cumulative probability function, μ is the median intensity measure of each damage state and β their reliability.

From these parameters, the median of the intensity measures (PGA, Arias-intensity) for each damage state can be calculated by inverting Eq. (5). by substituting the median displacement of the damage states, which can be calculated based on the intervals. Following this methodology, the median values for each damage state, embankment height, and intensity measures are shown in Table 7.

Table 5 Parameters of Eq. (5) describing the relationship between intensity and displacement

Embankment height (m)	PGA		Arias-intensity	
	α_{PGA}	β_{PGA}	α_{Arias}	β_{Arias}
9.0	3.7151	2.0004	0.2546	0.9225
6.0	1.5693	1.8526	0.1578	1.0045
3.0	0.9962	2.0384	0.0674	1.0017

Table 6 Damage states suggested by Argyroudis and Kaynia [6]

Structure type	Damage state	Peak ground displacement (PGD) [m]	
		min	max
Highway embankments	Small	0.02	0.08
	Medium	0.08	0.22
	Severe/Total	0.22	0.58

Table 7 Median intensity measures for three damage states

	Median PGA (g)			Median Arias-intensity (m/s)		
	Embankment height (m)					
Damage state	9.0	6.0	3.0	9.0	6.0	3.0
Small (DS1)	0.116	0.156	0.230	0.151	0.266	0.567
Medium (DS2)	0.201	0.282	0.395	0.481	0.782	1.767
Severe/ Total (DS3)	0.328	0.478	0.639	1.555	1.886	3.826

The reliability (β_D) of ground response analysis results can be quantified by the standard deviation of the seismic intensity parameters corresponding to the exceedance of a given damage state. The level of uncertainty in the damage states (β_{DS}) were taken as 0.4, as defined by HAZUS [23] for buildings. The uncertainties in the capacity of the structures (β_C) was taken as 0.3 after Argyroudis and Kaynia [6]. The total reliability of the structures can be defined as the square root of the sum of the squares of the individual uncertainties (Eq. (9)). The calculated total reliabilities for different embankment heights are shown in Table 8.

$$\beta_{tot} = \sqrt{\beta_{DS}^2 + \beta_C^2 + \beta_D^2} \tag{9}$$

Given the defined reliability parameters and median values, the fragility curves were constructed for each damage state using Eq. (8). Fig. 8. shows the probability of exceedance of each damage state with increasing peak ground acceleration. The fragility curves were defined based on PGA values between 0.05–0.35 g, therefore the fragility curves require extrapolation beyond this value and their accuracy are less certain. Similar fragility curves can be defined for Arias-intensity as base parameter, which are shown on Fig. 9.

On the basis of the defined fragility curves, the probability of exceeding different damage states can be estimated for a given seismic intensity and embankment heights. The curves can be developed from the two different intensity metrics (PGA and Arias-intensity) and show significant differences. This would imply that the curves are not equivalent to each other and should not be interchanged. While PGA characterizes the maximum ground acceleration, the Arias-intensity describes the energy of given earthquake.

Based on the fragility curves, a PGA = 0.35 g (standard for this site) there is over 90 % probability of exceeding the DS1 damage state for a 6m and 9m high embankment, while for a 3 m height it reduces to ~80 %. The 80 % probability corresponds to a DS2 damage state for a 9 m high embankment.

Table 8 Total reliabilities of each analysis

Total reliability for PGA(-)			Total reliability for Arias-intensity (-)		
Embankment height (m)					
9.0	6.0	3.0	9.0	6.0	3.0
0.64	0.54	0.52	0.52	0.53	0.54

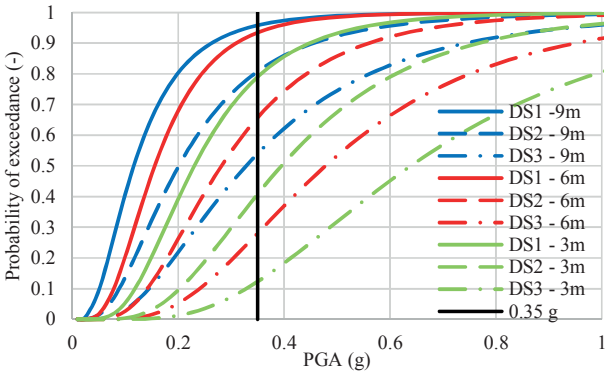

Fig. 8 Fragility curves defined for different damage states and embankment heights based on Arias-intensity

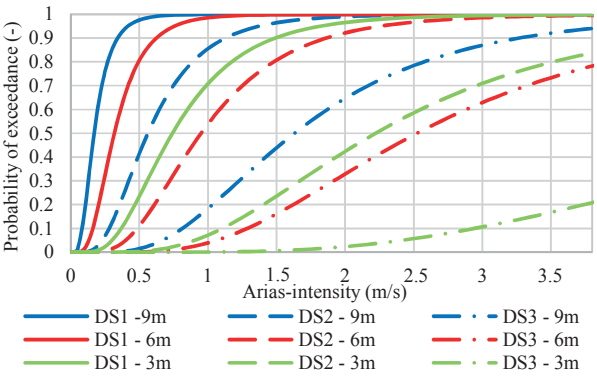

Fig. 9 Fragility curves defined for different damage states and embankment heights based on Arias-intensity

Fragility curves based on Arias-intensity (Fig. 9) show far greater dispersion for each damage class. They also show a wider distribution based on embankment height. Additional fragility curves based on Arias-intesity could be developed for embankment heights between 3–9 m using parameters chosen for Eq. (5) based on Fig. 7.

The resulting fragility curves approximate the probability of exceeding using a lognormal distribution function.

As a last step of the investigation, the fit of the discrete results of the 2-D model and the assumed lognormal fragility curves was examined.

Comparison of these for the case of the DS1 damage state for a 9 m high embankment is shown in Fig. 10(a). The deviation of the values of the PGA based DS1 fragility curve is shown in Fig. 10(b), which is closely matched to the defined values. Based on our experience, the vulnerability curves based on the Arias-intensity showed a better fit to the measured values. It is important to note, that the generated fragility curves do not always lead to a conservative approximation of the 2-D results, especially in case of relatively low probabilities.

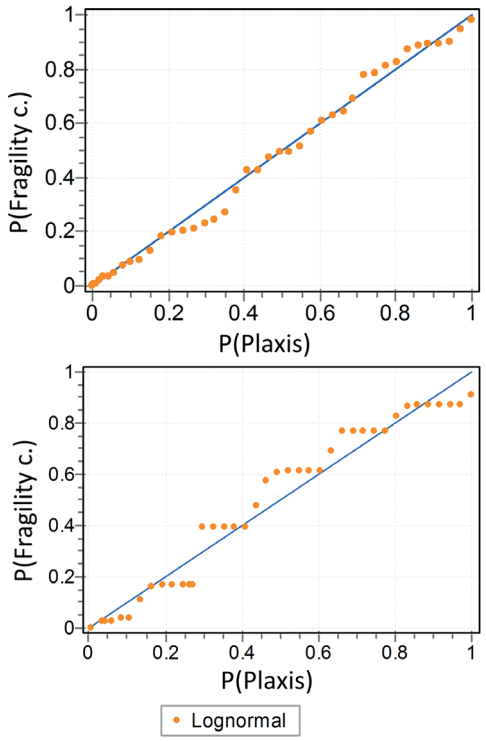

Fig. 10 Correlation of the probabilities based on the developed fragility curves and the discrete probabilities based on the Plaxis models a) based on Arias-intensity, b) based on PGA

3 Conclusions

1. We have demonstrated a method to develop fragility curves for embankments using 1-D and 2-D response analysis software. They can be used as planning tools for rescue and recovery and to help strengthen critical transportation lifelines in the case of an earthquake.
2. We have applied two different intensity measures, PGA and Arias-intensity. They produce markedly different results and should not be interchanged.
3. We have described the relationship between crown displacements and intensity measures with a power function. A stronger correlation between Arias-intensity and displacements was found compared to PGA values.
4. Fragility functions were developed based on the applied intensity measures. The curves based on the Arias-intensity showed a wider dispersion for each damage class.
5. The application of a lognormal distribution leads to non-conservative results in case of low probabilities, therefore care and engineering judgement should be exercised in these cases.

References

[1] Simon, J., Vigh, L. G., Horváth, A. "Magyarországi közúti hidak szeizmikus viselkedése és károsodáselemzése" (Seismic behaviour and damage analysis of hungarian roadway bridges), In: A BME Hidak és Szerkezetek Tanszék Tudományos Közleményei: Tass Géza és Orosz Árpád 90 éves, Budapest University of Technology and Economics, Budapest, Hungary, 2016, pp. 89–98. (in Hungarian) [online] Available at: http://real.mtak.hu/id/eprint/39995

[2] Katona, T. J. "Rendszerszintű döntések a Paksi Atomerőmű hosszú távú, biztonságos üzemeltetése érdekében" (Systemic decisions for the sake of long-term, safe operation of the Paks Nuclear Reactor), Thesis (Doctor of the Hungarian Academy of Sciences), Hungarian Academy of Sciences, 2011. (in Hungarian) [online] Available at: http://real-d.mtak.hu/id/eprint/425

[3] Ahmadi, M., Naderpour, H., Kheyroddin, A., Gandomi, A. H. "Seismic Failure Probability and Vulnerability Assessment of Steel-Concrete Composite Structures", Periodica Polytechnica Civil Engineering, 61(4), pp. 939–950, 2017. https://doi.org/10.3311/PPci.10548

[4] Rossetto, T., Elnashai, A. "Derivation of vulnerability functions for European-type RC structures based on observational data", Engineering Structures, 25(10), pp. 1241–1263, 2003. https://doi.org/10.1016/S0141-0296(03)00060-9

[5] Maruyama, Y., Yamazaki, F., Mizuno, K., Tsuchiya, Y., Yogai, H. "Fragility curves for expressway embankments based on damage datasets after recent earthquakes in Japan", Soil Dynamics and Earthquake Engineering, 30(11), pp. 1158–1167, 2010. https://doi.org/10.1016/j.soildyn.2010.04.024

[6] Argyroudis, S., Kaynia, A. M. "Analytical seismic fragility functions for highway and railway embankments and cuts", Earthquake Engineering & Structural Dynamics, 44(11), pp. 1863–1879, 2015. https://doi.org/10.1002/eqe.2563

[7] Permanent Committee of Revising the Code of Practice for Seismic Resistant Design of Buildings "Code No.2800 Iranian Code of Practice for Seismic Resistant Design of Buildings", 3rd eds., Building and Housing Research Center, Tehran, Iran, 2007.

[8] CEN "EN 1998-1:2004 Eurocode 8: Design of structures for earthquake resistance Part 1: General rules, seismic actions and rules for buildings", European Committee for Standardization, Brussels, Belgium, 2004.

[9] Pacific Earthquake Engineering Research Center "NGA-West 2 Ground Motion Database", [online] Available at: https://ngawest2.berkeley.edu/spectras/new?sourceDb_flag=1 [Accessed: 12 December 2018]

[10] Katona, T. J. "Atomerőművek földrengés utáni állapot-értékelésére szolgáló kár-indikátorok összehasonlító vizsgálata" (Comparison of damage-indicators for the analysis of nuclear reactors after earthquake), Nukleon, VI(2), Article number: 134, 2013. (in Hungarian) [online] Available at: https://nuklearis.hu/node/13

[11] Board of Trustees of University of Illinois at Urbana-Champaign, Hashash, Y. "DeepSoil (6.1)" [computer program] Available at: http://deepsoil.cee.illinois.edu/ [Accessed: 10 June 2019]

[12] Newmark, N. M. "A method of computation for structural dynamics", Journal of the Engineering Mechanics Division, 85(3), pp. 67–94, 1959.

[13] Darendeli, M. B. "Development of new family of normalized modulus reduction and material damping curves", PhD Thesis, University of Texas at Austin, 2001. [online] Available at: https://repositories.lib.utexas.edu/bitstream/handle/2152/10396/darendelimb016.pdf

[14] Bentley Systems Incorporated "On the use of dynamic boundary conditions" [online] Available at: https://communities.bentley.com/products/geotech-analysis/w/plaxis-soilvision-wiki/45984/on-the-use-of-dynamic-boundary-conditions

[15] Amorosi, A., Boldini, D., Elia, G. "Parametric study on seismic ground response by finite element modelling", Computers and Geotechnics, 37(4), pp. 515–528, 2010. https://doi.org/10.1016/j.compgeo.2010.02.005

[16] Vrettos, C. "Dynamic response of soil deposits to vertical SH waves for different rigidity depth-gradients", Soil Dynamics and Earthquake Engineering, 47, pp. 41–50, 2013. https://doi.org/10.1016/j.soildyn.2012.04.003

[17] Visone, C., Bilotta, E., Santucci de Magistris, F. "Remarks on site response analysis by using Plaxis dynamic module", Plaxis Bulletin, 23, pp. 14–18, 2008. [online] Available at: https://communities.bentley.com/products/geotech-analysis/w/plaxis-soilvision-wiki/46088/remarks-on-site-response-analysis-by-using-plaxis-dynamic-module

[18] Kuhlmeyer, R. L., Lysmer, J. "Finite Element Method Accuracy for Wave Propagation Problems", Journal of the Soil Mechanics and Foundation Division, 99(5), pp. 421–427, 1973.

[19] Benz, T. "Small-Strain Stiffness of Soils and its Numerical Consequences", PhD Thesis, Institute of Geotechnical Engineering, University of Stuttgart, 2007. [online] Available at: https://communities.bentley.com/products/geotech-analysis/w/plaxis-soilvision-wiki/46080/small-strain-stiffness-of-soils-and-its-numerical-consequences

[20] Brinkgreve, R. B. J., Kappert, M. H., Bonnier P. G. "Hysteretic Damping in a small-strain stiffness model", In: Proceedings of the 10th International Symposium on Numerical Models in Geomechanics (NUMOG X), Rhodes, Greece, 2007, pp. 737–742. https://doi.org/10.1201/NOE0415440271.ch106

[21] Hudson, M., Idriss, I. M., Beikae, M. "QUAD4M User's Manual", [pdf] Center for Geotechnical Modeling, Department of Civil and Environmental Engineering, University of California, Davis, CA, USA, 2003. Available at: https://www.researchgate.net/publication/288511774_QUAD4M_-_A_Computer_Program_to_Evaluate_the_Seismic_Response_of_Soil_Structures_Using_Finite_Element_Procedures_Incorporating_a_Compliant_Base

[22] Laera, A., Brinkgreve, R. B. J. "Ground Response analysis in PLAXIS", Bentley, Exton, PA, USA [pdf] Available at: https://www.plaxis.com/content/uploads/import/kb/kb-publications/PLAXIS_Ground_response_analysis.pdf

[23] FEMA "HAZUS-MH: User's Manual and Technical Manuals", [pdf] Federal Emergency Management Agency, Washington, DC, USA, 2009. Available at: https://www.researchgate.net/publication/332766615_HAZUS_R_-MH_Advanced_Engineering_Building_Module_AEBM_Technical_And_User's_Manual_Developed_by_Federal_Emergency_Management_Agency

[24] Argyroudis, S., Kaynia, A. M. "Fragility Functions of Highway and Railway Infrastructure", In: Pitilakis, K., Crowley, H., Kaynia, A. M. (eds.) SYNER-G: Typology Definition and Fragility Functions for Phisical Elements at Seismic Risk, Springer, Dordrecht, Netherlands, 2014, pp. 299–325. https://doi.org/10.1007/978-94-007-7872-6